

www.acsami.org Research Article

Nanoporous Atomically Thin Graphene Filters for Nanoscale Aerosols

Peifu Cheng, Jeremy Espano, Andrew Harkaway, Andrew E. Naclerio, Nicole K. Moehring, Philipp Braeuninger-Weimer, and Piran R. Kidambi*



Cite This: ACS Appl. Mater. Interfaces 2022, 14, 41328–41336



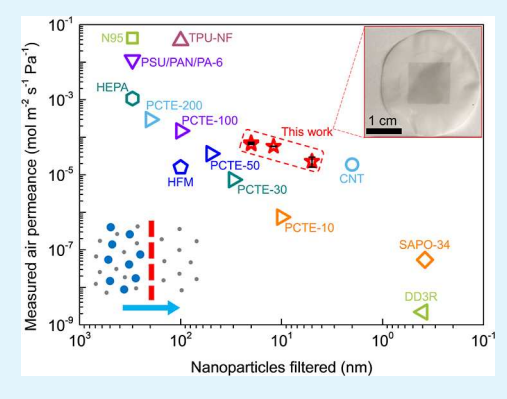
ACCESS I

III Metrics & More

Article Recommendations

SI Supporting Information

ABSTRACT: Filtering nanoparticulate aerosols from air streams is important for a wide range of personal protection equipment (PPE), including masks used for medical research, healthcare, law enforcement, first responders, and military applications. Conventional PPEs capable of filtering nanoparticles <300 nm are typically bulky and sacrifice breathability to maximize protection from exposure to harmful nanoparticulate aerosols including viruses $\sim 20-300$ nm from air streams. Here, we show that nanopores introduced into centimeter-scale monolayer graphene supported on polycarbonate track-etched supports via a facile oxygen plasma etch can allow for filtration of aerosolized SiO₂ nanoparticles of $\sim 5-20$ nm from air steams while maintaining air permeance of $\sim 2.28-7.1 \times 10^{-5}$ mol m⁻² s⁻¹ Pa⁻¹. Furthermore, a systematic increase in oxygen plasma etch time allows for a tunable size-selective filtration of aerosolized nanoparticles. We demonstrate a new route to realize ultra-compact, lightweight, and conformal form-factor filters capable of blocking sub 20 nm aerosolized nanoparticles with particular relevance for bioless with particular relevance for bioless.



of blocking sub-20 nm aerosolized nanoparticles with particular relevance for biological/viral threat mitigation.

KEYWORDS: filtering nanoscale aerosols, graphene membranes, virus filtration, nanoporous atomically thin membranes, personal protective equipment, nanopores

■ INTRODUCTION

Airborne nanoparticles¹⁻⁹ include pollutants, toxins, engineered nanoparticles, and infectious/harmful viruses (~20-300 nm in diameter), such as the influenza virus, rhinovirus, and coronavirus, among others. Most conventional air filters, 14-16 for example, the high-efficiency particulate air filter (HEPA) and the non-oil 95% efficiency filter (N95) have excellent air flow rates ($\sim 1.08 \times 10^{-3}$ to 4.40×10^{-2} mol m⁻² s⁻¹ Pa⁻¹)^{14,15} but struggle to filter nanoparticles <300 nm. State-of-the-art personal protective equipment (PPE), for example, masks capable of filtering nanoparticles <300 nm and specifically in the lower size ranges (<100 nm) remain bulky and cumbersome to use and, in most cases, create thermal stress due to poor breathability; 17 that is, they do not allow for sweat-based cooling via rapid water vapor transport. 18 However, PPEs with efficient evaporative cooling of the human body through perspiration are highly desired in protective applications for medical research, healthcare, law enforcement, first responders, and military applications.

Approaches to develop improved PPEs have mostly focused on making porous polymers with high thicknesses where nanoparticulate pollutants, toxins, or pathogens are removed by depth filtration. However, these approaches do not guarantee protection since longer exposure will inevitably lead to a break-through and the breathability for such thick polymer layers is typically very low. To Some progress has indeed been

made in increasing breathability of conventional polymeric materials; for example, (i) by introducing porosity in butyl rubber-based materials¹⁹ and developing reactive organic/ inorganic composite film materials that actively degrade harmful agents on contact,²⁰ (ii) including non-woven materials, 21 (iii) fabricating hollow fiber membrane by spinning polymers (air permeance of $\sim 1.6 \times 10^{-5}$ mol m⁻² s⁻¹ Pa⁻¹, filtration size 100 nm),²² (iv) incorporating Li⁺ ions in thermoplastic polyurethane nanofiber/net (TPU-NF) membrane-based air filters (air permeance of $\sim 3.7 \times 10^{-2}$ mol m⁻² s⁻¹ Pa⁻¹, filtration size 100 nm, PM_{0.1}),²³ and (v) integrating microfiber layers of polysulfone (PSU), polyacrylonitrile (PAN) nanofiber layer, and polyamide-6 (PA-6) nets to build the PSU/PAN/PA-6 air filter (air permeance of ~1.2 \times 10⁻² mol m⁻² s⁻¹ Pa⁻¹, filtration size \sim 300 nm NaCl aerosol particles).²⁴ Finally, etching nanoscale tracks in polymers have also been explored; for example, polycarbonate track-etch (PCTE) membranes with different pore sizes ~10-200 nm

Received: June 17, 2022 Accepted: August 15, 2022 Published: August 29, 2022





© 2022 American Chemical Society

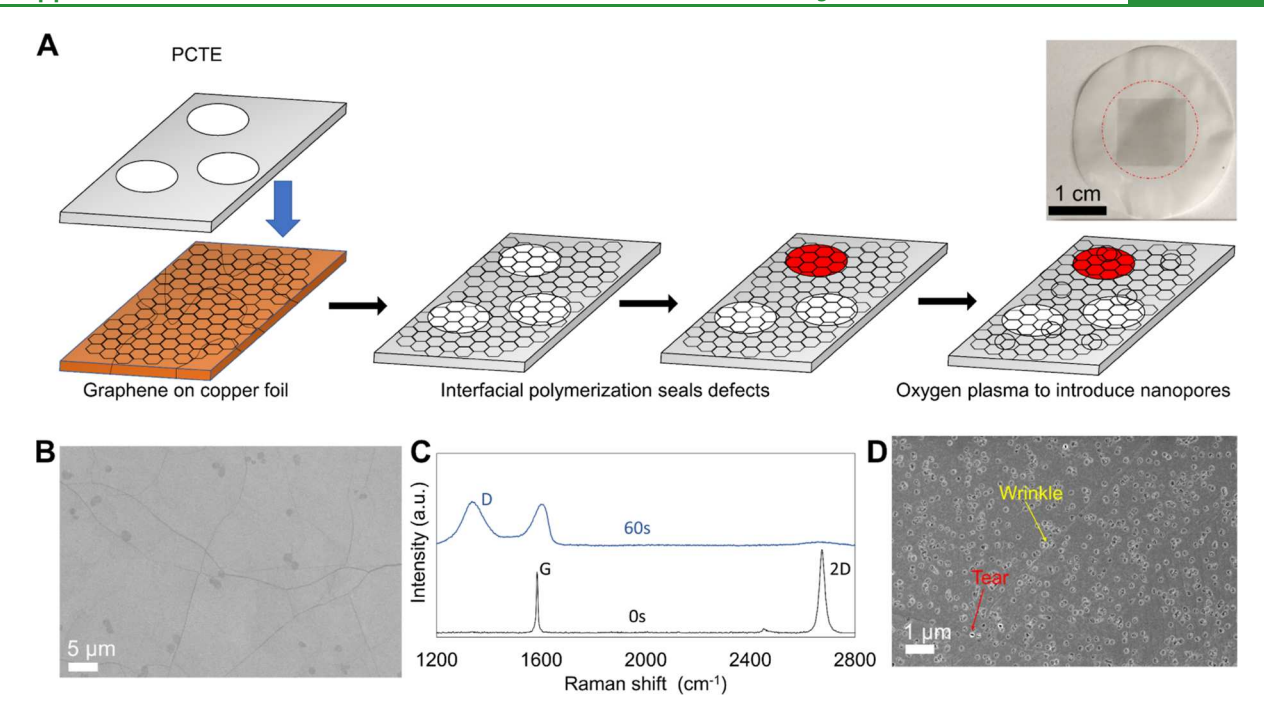


Figure 1. (A) Schematic of the fabrication process for atomically thin graphene membranes supported on polycarbonate track-etched (PCTE) supports. Inset shows an optical image of the graphene membrane. Dark square represents graphene, and the red circle represents the area where interfacial polymerization (IP) was performed. SEM image of (B) as-synthesized CVD graphene on copper foil and (D) CVD graphene after transfer to PCTE supports. (C) Raman spectrum of CVD graphene on 300 nm SiO_2/Si wafer before and after 60 s of oxygen plasma etch. The increase in D peak after plasma etch confirms the formation of defects in the graphene lattice.

show air permeance from ${\sim}7.4\times10^{-7}$ to 3×10^{-4} mol m $^{-2}$ s $^{-1}$ Pa $^{-1}.^{25}$

In this context, membranes incorporating nanomaterials such as vertically aligned carbon nanotubes (CNTs) with <5 nm diameter have shown nitrogen permeance of 1.81 \pm 0.36 \times 10⁻⁵ mol m⁻² s⁻¹ Pa⁻¹, as well as the ability to block 3 nm charged dyes, 5 nm uncharged gold (Au) nanoparticles, and ~40–60 nm dengue virus from aqueous solutions. 26 Vertically aligned CNT membranes with <2 nm pores have also shown air permeance $\sim 1.9 \times 10^{-5}$ mol m⁻² s⁻¹ Pa⁻¹ attributed to slip length and the atomically smooth CNT surfaces.²⁷ However, tuning CNT diameters to target specific applications requiring filtration of aerosolized nanoparticles of a particular size and scaling-up for large-area manufacturing remains challenging. More recently, theoretical calculations have suggested porous silicon membranes for protection against corona viruses.²⁸ Finally, zeolite membranes have also shown high permeance; for example, the decadodesil 3R (DD3R) membrane has air permeance of $\sim 2.2 \times 10^{-9}$ mol m⁻² s⁻¹ Pa⁻¹ with pores $\sim 0.36 \times 0.44$ nm,²⁹ while the silicoaluminophosphate-34 (SAPO-34) membrane shows air permeance of ~5.4 \times 10⁻⁸ mol m⁻² s⁻¹ Pa⁻¹ with a pore size of ~0.38 nm but has not been tested for aerosol filtration.3

Graphene with atomic thinness, high mechanical strength, 31 chemical robustness, and high-density nanopores presents a new class of materials for size-selective separation. 32,33 Here, we demonstrate a novel approach to develop nanoporous atomically thin graphene membranes for filtering nanoscale aerosols $\sim 5-20$ nm (SiO₂ nanoparticles) from air streams while maintaining up to $\sim 7.12 \times 10^{-5}$ mol m⁻² s⁻¹ Pa⁻¹ ($\sim 75\%$ of the air flow of the bare substrate). The ultracompact, lightweight, and conformal form-factor filters offer transformative advances for PPE for medical research, healthcare, law enforcement, first responders, and military

applications. To the best of our knowledge, this is one of the first demonstrations of an atomically thin membrane filtering aerosolized nanoparticles in the \sim 5–20 nm size range.

■ RESULTS AND DISCUSSION

A schematic of our fabrication process and an optical image of the resulting centimeter-scale nanoporous graphene membrane are shown in Figure 1A. Monolayer graphene synthesized via chemical vapor deposition (CVD) on copper foil 34,35 is initially transferred onto PCTE supports with $\sim\!200$ nm pores, and any large tears are sealed by interfacial polymerization (IP) before introducing nanopores via an oxygen plasma etch (0–180 s) of the graphene lattice (see Experimental Section). $^{34-43}$

Scanning electron microscopy (SEM) image (Figure 1B) of the as-synthesized CVD graphene on Cu foil shows wrinkles (originating from the differences in thermal expansions of graphene and copper), indicating a continuous layer. Raman spectroscopy (Figure 1C) with the characteristic graphene peaks (2D \sim 2700 cm⁻¹, $G \sim$ 1600 cm⁻¹) and the absence of a D peak (\sim 1350 cm⁻¹) confirms the high quality of the synthesized monolayer ($I_{\rm 2D}/I_{\rm G} > 1$) graphene film. The SEM image of graphene on PCTE support (Figure 1D) shows a majority of PCTE pores with \sim 200 nm diameter covered with graphene (darker contrast in SEM), indicating successful transfer, along with some uncovered regions (brighter regions in SEM) due to tears in the graphene from the manual pressing step of the transfer. These uncovered regions in the PCTE appear brighter in the SEM due to polymer charging (Figure 1D).

The well-defined cylindrical geometry of the PCTE support avoids interconnected pores and thereby (i) enables sealing of tears and other macroscopic damage/defects to graphene from transfer via IP and (ii) also allows for clear interpretation of transport results from the atomically thin graphene layer.³²

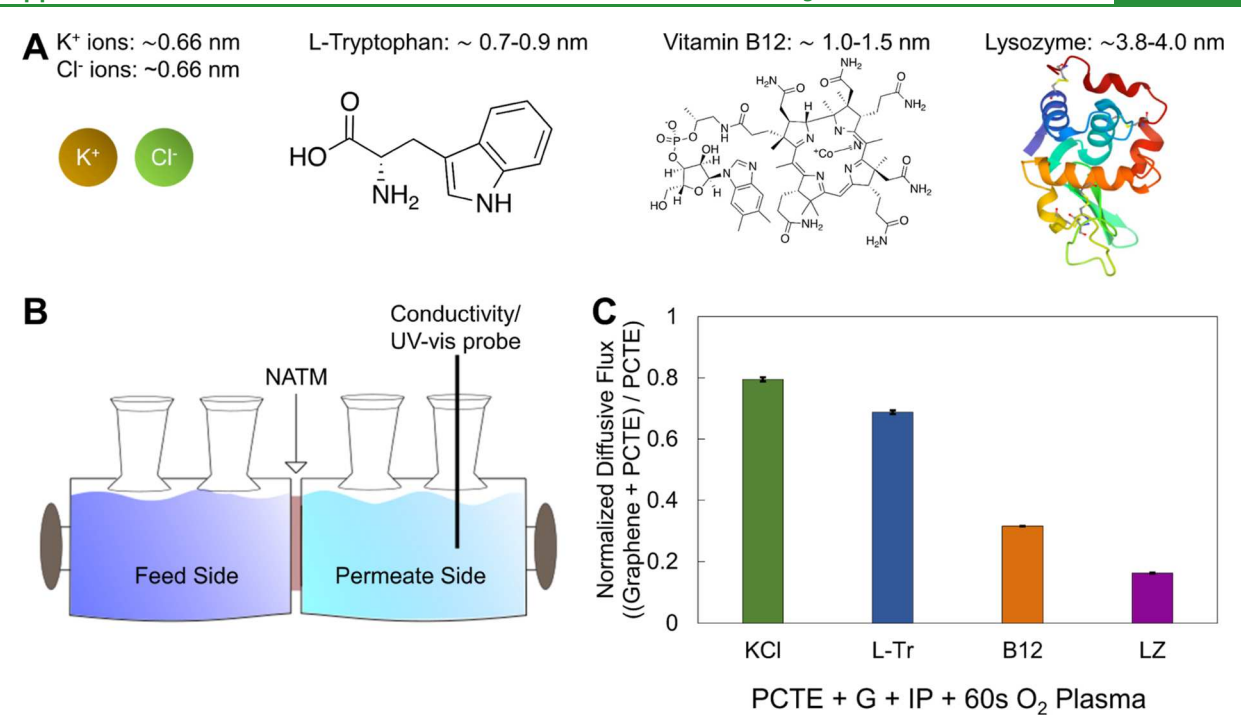


Figure 2. (A) Schematics of salts and small molecules used in the diffusion-driven flow measurements. Lysozyme image adapted with permission from ref 60 RCSB PDB (rcsb.org) of PBD ID 2LYM (C. E. Kundrot and F. M. Richards, *J. Mol. Biol.*, 1987, 193, 193, 1). (B). Schematic of the setup used to measure diffusion-driven flow through the graphene membranes. (C) Normalized diffusive flux with respect to bare PCTE ((PCTE+G)/PCTE) through atomically thin membranes. Lysosomes \sim 3.8–4.0 nm exhibit the lowest transport and hence maximum rejection, indicating that the majority of nanopores introduced into the graphene membranes are <4 nm.

Specifically, the IP process^{38,41,46,47} used to seal tears and other damages/large defects from graphene transfer leverages (i) the immiscibility of hexane and water to form a sharp interface, (ii) the solubility of trimesoyl-chloride solution (TMC) in hexane and its instability (decomposition) in water, and (iii) the solubility of octa-ammonium-polyhedral-oligomeric-silsesquioxane (POSS) in water and its insolubility in hexane. Hence, the interface for the formation of IP plugs is pinned within the PCTE support pore (since TMC will dissociate in water, POSS will have to diffuse into the organic phase to react with TMC and form a plug), thereby allowing the graphene surface to remain clean. 46,48,49 Post IP, nanopores are introduced via the facile plasma etch of the graphene lattice (see Experimental Section) before testing the membranes. 50,51 The Raman spectrum of graphene subjected to oxygen plasma (60 s) confirms the formation of defects (see the large D peak in Figure 1C). 38,45

Initially, we characterized the nanopores introduced into the graphene membranes by measuring diffusion-driven flow of ions and molecules, representing sizes from ~0.66 to 4 nm (Figure 2A), that is, KCl (hydrated K⁺ and Cl⁻ ions ~0.66 nm), L-tryptophan (L-Tr, ~0.7-0.9 nm), vitamin B12 (B12, ${\sim}1{-}1.5$ nm), and lysozyme (Lz, ${\sim}3.8{-}4.0$ nm) using a sideby-side diffusion cell (Figure 2B). 32,38 Representative diffusiondriven flow measurements through graphene membranes subjected to 60 s of oxygen plasma time (PCTE + G + IP + 60s O₂ plasma) show a flux of KCl > L-Tr > B12 > Lz. The normalized diffusive flux with respect to a bare PCTE membrane (Figure 2C) for KCl ~79.5%, L-Tr ~68.8%, B12 ~31.6%, and Lz ~16.3% indicates the majority of the nanopores introduced into the graphene lattice are <4 nm (for 60 s of oxygen plasma), consistent with prior observations in the literature.³⁸ These observations indicate that nanopores

in our atomically thin graphene membranes allow for the size-selective transport of smaller ions and molecules such as KCl, L-Tr, and B12 while hindering the transport of larger macromolecules such as Lz ~3.8–4 nm.^{32,38,52} Diffusion-driven flow measurements for molecules >4 nm in diameter are non-trivial, wherein the slow diffusion of the larger molecules can influence measurements.

Next, we mounted the graphene membranes into our custom-built setup (Figures 3C and S1) to evaluate the performance of the graphene membranes for filtering aerosolized nanoparticles with SiO₂ as a model system. We note that Boutilier et al. used a similar setup to measure gas flow through nanoporous atomically thin membranes.⁵³ A perforated steel plate was used to provide mechanical stability to the membranes over centimeter-scale areas experiencing differential pressure, and an aluminum masking tape with a 5 mm hole and epoxy on the edges was used to define the area of measurement (Figure 3A,B) as well as prevent leakages.

The rate of pressure change in the evacuated reservoirs in the setup was used to measure the air flow through graphene membranes (Figure 3D). The large reservoir, system base pressure ~2–3 Torr with a roughing pump, and the high accuracy of the pressure transducer allowed for a linear relationship between pressure change and time even for the maximum flows measured in our experimental design, that is, bare steel supports (~2800 mTorr/s, Figures S2–S4). We also minimized variations in the base pressure at the start of the experiments (~2–3 Torr) to mitigate any influence on the measurements (Figures S3 and S4). The upper bound of air flow that can be achieved with our graphene membrane in this study is the air flow corresponding to the rate of change in pressure through a bare PCTE (~10% porosity) support without graphene ~13.47 mTorr/s. We emphasize that

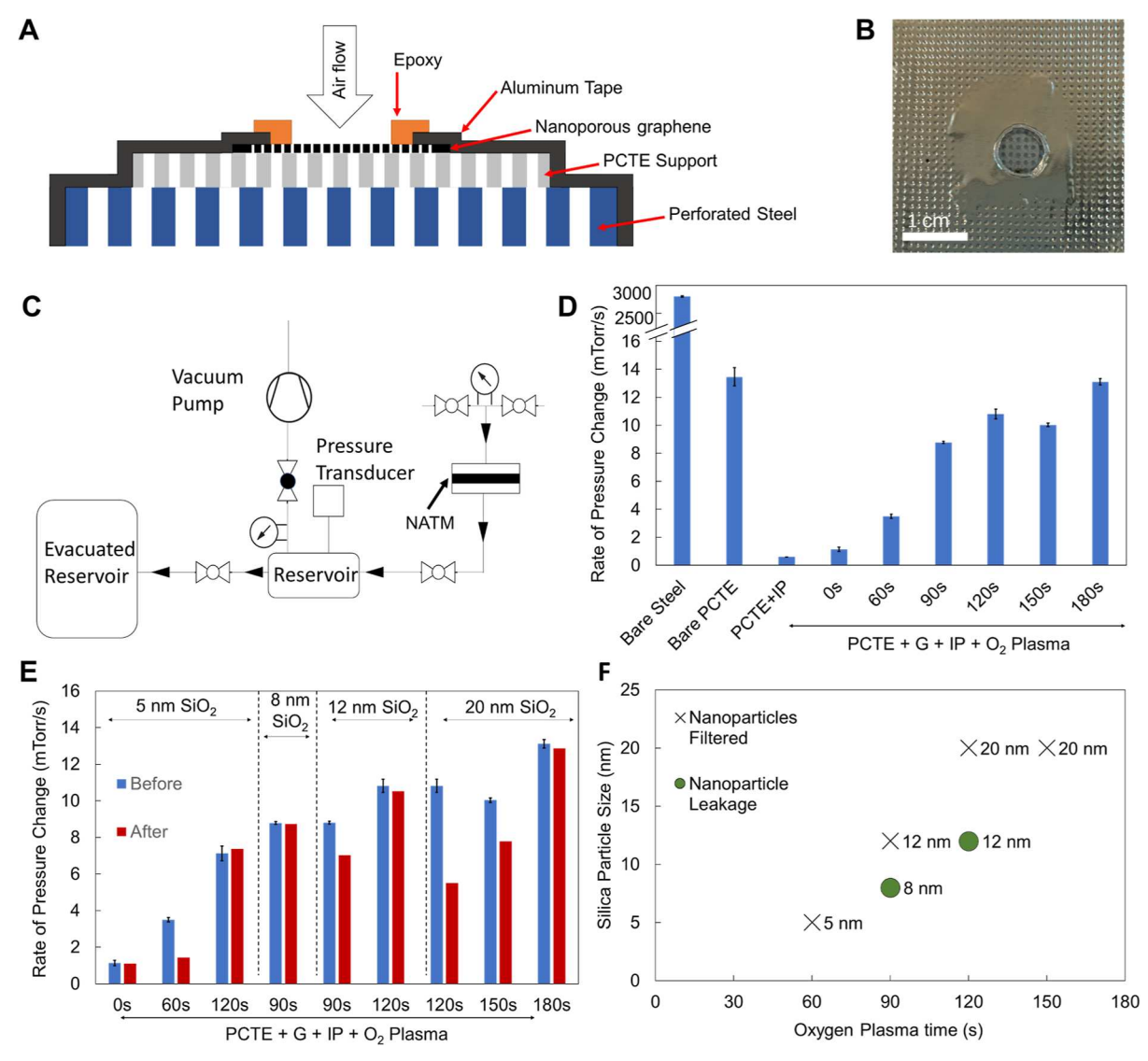


Figure 3. (A) Schematic of the cross-section and (B) optical image (top view) of the atomically thin graphene membrane mounted onto a perforated steel support using aluminum tape with a hole punched into it. (C) Schematic of the experimental test rig. (D) Rate of pressure change (indicating transport of air) measured for different membranes. An increase in oxygen plasma time results in an increase in the rate of pressure change for graphene membranes. (E) Comparison of the rate of pressure change before (blue) and after (red) testing the graphene membranes with aerosolized silica nanoparticles. A reduction in the rate of pressure change indicates blockage of the nanopores due to silica nanoparticles. Error bars in (D,E) indicate one standard deviation. (F) Blockage of silica nanoparticles as a function of oxygen plasma time for graphene membranes.

increasing support porosity and support pore diameter as well as reducing support thickness will allow for much higher air permeances and can be pursued for practical applications in future developments.

Bare PCTE membranes subjected to IP showed a rate of change in pressure $\sim\!0.60$ mTorr/s, which indicates a lower bound on air flow through the membranes and indicates baseline leakage through IP plugs. Interestingly, graphene transferred to PCTE and treated with IP (PCTE + G + IP) showed a rate of change in pressure of $\sim\!1.10$ mTorr/s (Figure 3D). These observations indicate that graphene can withstand the pressure difference between the evacuated chamber $\sim\!2.50$ Torr and ambient pressure 54 in agreement with literature reports, wherein single layer graphene supported on PCTE supports was shown to withstand pressure differences of up to 100 bar. The rate of pressure change for PCTE + G + IP $\sim\!1.10$ mTorr/s is comparable to the baseline leakage rate of

0.40 mTorr/s (see Figure S2) indicating that the PCTE + G + IP membrane without nanopore creation allows for negligible air flow. Hence, we introduced nanopores via facile oxygen plasma etch and observed an increase in the rate of change in pressure values to ~ 3.50 and ~ 8.78 mTorr/s for 60 and 90 s of etch times, respectively. Extending the oxygen plasma time further increases the rate of pressure change until a value of ~ 13.11 mTorr/s is reached for 180 s of etch time, that is, similar to the PCTE support value of ~ 13.47 mTorr/s, indicating extensive structural damage to the graphene lattice in agreement with prior studies using oxygen plasma to etch graphene. The variability between membranes (e.g., PCTE + G + IP + 120 s O₂ plasma and PCTE + G + IP + 150 s O₂ plasma) stems from different graphene transfer yields, IP processes, and epoxy sealing.

Having measured the rate of change of pressure as a function of oxygen plasma etch time on our graphene membranes, we proceeded to evaluate their ability to filter aerosolized nanoparticles using SiO₂ as a model system in air streams. We selected silica aerosols because the silica particles are rigid spheres with a very narrow size distribution, for example, 5 nm silica (\sim 4–6 nm), 8 nm silica (\sim 7–10 nm), 12 nm silica $(\sim 10-14 \text{ nm})$, and 20 nm silica $(\sim 20 \text{ nm})$ and are inexpensive. The extremely narrow particle size distribution and rigid sphere geometry make them ideal model systems for probing defect sizes in our graphene membranes. The SiO₂ nanoparticles of a specific size (5, 8, 12, or 20 nm) were aerosolized from 0.6 mL (15 to 40 wt % in H₂O) of colloidal dispersions and allowed to mix with the air stream that passes through our graphene membranes (Figures 3C and S1). We compared the rate of change of pressure for the membranes before and after they were exposed to the aerosolized SiO₂ nanoparticles in the air stream (Figure 3E,F). Any decrease in flow rate for the same membrane after exposure to the aerosolized nanoparticles indicates filtering of the nanoparticles via plugging of the etched nanopores (Figure 3E,F). 55,56 The concentration of SiO₂ nanoparticles was deliberately kept low enough to rule out the formation of a nanoparticulate filter cake/coating on our graphene membranes (see Figure S7). Furthermore, we emphasize that the formation of a filter cake will reduce the rate of change of pressure for all graphene membranes, irrespective of the size of particles being tested, and such an effect was not seen in our experiments (see Figure 3 and Figure S7).

For the unetched graphene membrane (PCTE + G + IP + 0s O₂ plasma etch), the rate of change of pressure remains the same before and after testing with 5 nm SiO₂ nanoparticles (Figure 3E,F). The small rates of pressure change ~1.10 mTorr/s close to the system baseline leakage rate ~0.40 mTorr/s (Figure S2) indicate negligible airflow through the PCTE + G + IP + 0 s O₂ plasma membrane without the formation of nanopores. However, for graphene membranes subjected to 60 s etch, a distinct change is seen in the rate of pressure change before and after testing with 5 nm SiO₂ nanoparticles, indicating that the nanopores are blocked by the ~5 nm particles, which leads to them being filtered out (Figure 3E,F). We note that such an interpretation is also consistent with the diffusion-driven flow experiments (Figure 2C), where the graphene membranes etched for 60 s showed very low transport of Lz \sim 3.8-4nm. Notably, we did not see an increase in flow due to damage to the graphene from the SiO2 nanoparticles.

Increasing the O₂ plasma to 90 s shows no change in rate of pressure for ~5 and ~8 nm particles but shows an apparent change for \sim 12 nm particles. Further increase in O₂ plasma time to 120 s shows no change for ~12 nm particles, but the same membrane shows a change in rate of pressure for ~20 nm particles (Figure 3E,F). Finally, some reduction in rate of change in pressure is also observed for ~20 nm particles with 150 s of O₂, albeit not as significant as for 120 s, which is consistent with prior reports that showed oxygen plasma etching can increase pore size and pore density and that grain boundaries as well as pre-existing defects in graphene can etch at a faster rate than the formation and subsequent enlargement of new defects in the lattice. 38,39,53 We note that the graphene membranes subjected to 120 s of O2 plasma filter ~20 nm particles while exhibiting air permeance of $\sim 7.04 \times 10^{-4}$ mol m^{-2} s⁻¹ Pa⁻¹ (~75% of air flow of the bare PCTE support). We show that increasing oxygen plasma time results in a larger size of SiO₂ nanoparticles being blocked (Figure 3E,F). Hence,

the track-etched membranes do not completely dominate transport since we see clear differences with increasing oxygen plasma time that result in larger defects in graphene. Taken together, these experiments demonstrate the ability of nanoporous atomically thin graphene membranes to effectively filter aerosolized nanoparticles ~5-20 nm from air streams while maintaining high air flow. We note that the performance of our membranes can be further increased by using supports with larger pores, higher pore density, and lower thickness.

When comparing our NATM's performance to that of conventional membranes, our results exhibit the ability to block smaller nanoparticles than conventional filters (N95 filter, HEPA filters, TPU-NF). 14,15,23,27,57,58 Conventional membranes, such as N95 filters and HEPA filters, have both shown very high rates of permeance (\sim 4.40 \times 10⁻² to 1.08 \times 10⁻³ mol m⁻² s⁻¹ Pa⁻¹) but both show permeation of particles <300 nm (HEPA particles show permeation of pollen, dust, and smoke with sizes of 300 nm and smaller, and N95 filters show salt particle permeation below 300 nm). 14,15,57,58 As shown in Figure 4, our membranes allow for filtering aerosols

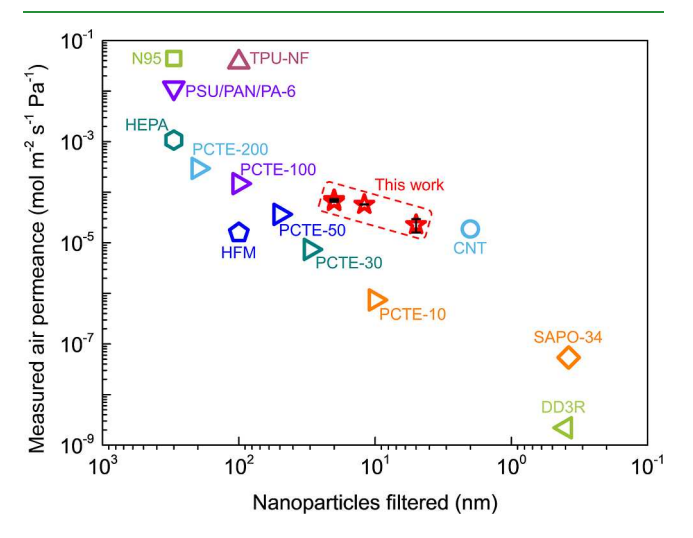


Figure 4. Measured air permeance as a function of the size of nanoparticles filtered using graphene membranes in this work (red stars) compared to commercial air filters like N95, 14 HEPAs, 15 PCTE membranes with different pore sizes (10-200 nm),25 and prior reported membranes in the literature, such as PSU/PAN/PA-6 air filter, ²⁴ TPU-NF, ²³ hollow-fiber membranes, ²² CNT membranes, ²⁷ SAPO-34 membrane,³⁰ and DD3R membrane.²⁹ All air permeance values are measured without taking into account the membrane porosities. Error bars indicate one standard deviation. Also see Figure S5.

in the \sim 5-20 nm range, along with permeance of \sim 7.04 \times 10⁻⁴ mol m⁻² s⁻¹ Pa⁻¹. Conventional membranes are unable to filter aerosols <300 nm but show much higher permeance, while the CNT membranes allow for blockage of ~2 nm particles but with lower permeance than the atomically thin nanoporous graphene membranes.²⁷ Taken together, these observations suggest that our graphene membranes can allow for access to a region in the parameter space which has remained inaccessible for conventional materials (Figure S5) but is highly desirable for PPE for a range of applications in healthcare, defense, and beyond.

CONCLUSIONS

In summary, we demonstrate atomically thin graphene membranes that are able to filter \sim 5-20 nm particles while maintaining an air permeance of up to $\sim 7.04 \times 10^{-4}$ mol m⁻² s^{-1} Pa⁻¹ (~75% of air flow as that of PCTE supports with 200 nm pores). Furthermore, the facile oxygen plasma etch of the graphene lattice allows for increasing the pore size to selectively filter larger nanoparticles. To the best of our knowledge, this is the first demonstration of an atomically thin membrane which filters nanoparticles in the \sim 5-20 nm size range. We anticipate that the development of such atomically thin membranes will allow access to a region in the parameter space that has remained inaccessible with conventional materials and will help enable compact, lightweight, and conformal form factors for applications in medical research, healthcare, space, defense, and beyond.

EXPERIMENTAL SECTION

Graphene Growth. Graphene growth on Cu foil (purity 99.9%, thickness 18 μ m, JX Holding HA) was performed by low-pressure CVD as previously reported. ^{34,35,38,39} Surface contaminants on the copper foil were initially removed by sonicating the foil in 15-20% nitric acid, followed by a rinse in de-ionized (DI) water, and dried in air. 34,35,38,39 Next, the foil was loaded into a hot-walled tube furnace heated to 1060 °C under 100 sccm of H2 and annealed for 60 $\mbox{min}^{34,35,38,39}$ Subsequently, graphene growth was initiated by adding 1 sccm of CH₄ to 100 sccm of H₂ for 30 min, followed by 2 sccm of CH₄ with 100 sccm of H₂ for 30 min^{34,35,38,39} Finally, the foil was quench cooled in the growth atmosphere.

Graphene Transfer to PCTE Supports. The graphene on the bottom side of the copper foil was removed by floating the foil in ammonium persulfate (APS, 0.2 M, Thermo Scientific, AC401160020) solution for 30 min, followed by DI water for 10 min, and dried in air. $^{34-39}$ The graphene on top of the copper foil was then pressed against polycarbonate track-etched (PCTE) support membranes (Sterlitech Corporation, 10 µm thick, polyvinylpyrrolidone-free, hydrophobic, 200 nm cylindrical pores, 10% porosity) .40-43 Next, copper was etched by floating the PCTE/graphene/Cu stack on APS solution.⁵⁹ The PCTE/graphene stack was finally rinsed by floating it on DI water, followed by a dip in ethanol (200 proof, Fisher Scientific, BP28184), and dried in air.

Graphene Transfer to SiO₂/Si Wafer. Graphene on Cu foil was pre-etched in APS solution as described above. Next, ~2 wt % solution of polymethyl methacrylate (PMMA, ACROS, 178760250) in anisole (Beantown Chemical, 130230) was drop-cast on the graphene on the top side of the Cu foil and allowed to dry. The Cu foil was then etched in APS solution, and the PMMA/graphene stack was rinsed in DI water and scooped onto a SiO₂ (300 nm)/Si wafer and dried at 50-80 °C for ~1 h before dissolving the PMMA in acetone and rinsing in isopropanol (IPA, Fisher Chemical, A416P-4).

Interfacial Polymerization. IP was carried out using octaammonium-POSS (Hybrid Plastics, AM0285) solution (0.4 g of POSS in 20 mL of DI water with a pH of 10.7 by adding NaOH) and trimesoyl-chloride (TMC, Alfa Aesar, 4422-95-1) solutions [0.035 g TMC in 10 mL hexane (VWR, BDH1129)] as previously reported. ^{34,35,38,39,41} Initially, the graphene/PCTE stack was placed on a glass slide on a hot plate at 105 °C for ~12 h³⁸ and subsequently sandwiched between Franz cells (PermeGear, Inc., 0.9 cm diameter orifice) with TMC and POSS solutions filled in the top and bottom cells, respectively, and left to react for 1 h. After IP, the membranes were rinsed with hexane and ethanol on the TMC side, unclamped, and rinsed in ethanol.

Oxygen Plasma Etching. Oxygen plasma etching was performed using a Harrick Plasma system (PDC-001) using pulses (15 s plasma etching followed by a 120 s pause) with an RF power of 7 W under 500 mTorr oxygen pressure to create nanopores in graphene membranes.

SEM and Raman Spectroscopy. SEM images of graphene on copper and graphene on PCTE supports were obtained using a Zeiss Merlin SEM with a Gemini II column operated at 2-5 kV.

Raman spectra for graphene were obtained on samples transferred to SiO₂/Si substrates using a Thermo Scientific DXR confocal Raman microscope with a 532 nm laser source.

Evaluating Graphene Membrane Performance. The graphene membranes on PCTE were placed on a perforated steel plate with 0.6 mm diameter holes and clamped via an aluminum tape with a 5 mm diameter hole punched in the center (Figure 3A) and loaded into the custom-built test ring. Epoxy was used to seal the edges of the hole punched in the aluminum tape to minimize any leakage.

Our custom-built test rig/setup (Figures 3C and S1) consisted of a 60-gallon vacuum chamber connected to a 3-gallon chamber with a pressure transducer (Omega, model number: PX409-015AUSBH) and a vacuum pump.⁵³ The graphene membrane was mounted into the system and sealed with flanges and gaskets, allowing for consistent experiments (see Figures S2-S4 for baseline leakage rates and measured flow rates). After mounting the membrane into the setup, the 60 and 3 gallon chambers were evacuated using a vacuum pump (Edwards RV5) until a base pressure of ~2.5 Torr was reached. Next, air flow through the membrane was measured by monitoring the pressure increase (Δ pressure, mTorr/s) for 60 s in the system by opening the valve connecting the 3-gallon tank to the membrane holder. Tests were performed in triplicates.

Filtration of aerosols was tested using various aerosolized silica particles (Nyacol Nano Technologies, ~15-40 wt % in water, https://www.nyacol.com/products/silicon-dioxide/). Silica aerosols have a particle size distribution as follows: 5 nm silica (\sim 4–6 nm), 8 nm silica (\sim 7–10 nm), 12 nm silica (\sim 10–14 nm), and 20 nm silica (~20 nm). Initially, air flow through each membrane was measured without silica particles. Next, silica particles were introduced into the air stream by aerosolizing 0.6 mL of silica particle solution with a specific particle size and allowing the aerosol to pass through the graphene membranes. The rate of change in pressure before and after introducing silica particles was compared. Separate membranes with identical pre-processing were used for each of the silica nanoparticle

Diffusion-driven flow of salts and small organic molecules in the liquid phase was measured as described elsewhere. 34,39,47,59 The membrane was sandwiched between two side-by-side diffusion cells (PermeGear Inc., 5 mm orifice, 7 mL volume) with graphene facing the feed side and rinsed with ethanol, followed by DI water. Next, the diffusion of KCl, L-tryptophan, vitamin B12, and lysozyme was measured in separate experiments, and magnetic stir bars were used to vigorously stir the feed and permeate side solutions.

Diffusion-driven transport of KCl was measured by introducing 0.5 M solution of KCl (Fisher Chemical, 7447-40-7 in the feed side with DI water in the permeate side, and the increase in conductivity of the DI water as a function of time was recorded with a conductivity meter (Mettler Toledo SevenCompact S230). The slopes of the curves from 10 min to 15 min were used to calculate the normalized flux for KCl flow rate across PCTE + G + \underline{IP} + $\underline{O_2}$ plasma flow rate across PCTE

For diffusion-driven flow of L-tryptophan (L-Tr, VWR, 73-22-3), vitamin B12 (B12, Sigma-Aldrich, 68-19-9), and lysozyme (Lz, VWR, 0663), 1 mM of solute in 0.5 M KCl solution was introduced into the feed side of the diffusion cell with 0.5 M KCl solution added to the permeate side. A fiber optic dip probe attached to a UV-vis spectrometer (Agilent, Cary 60) was immersed into the permeate side to monitor the change in concentration (absorbance change in the range of 190-1100 nm was measured every 15 s for 40 min). The UV-vis intensity differences between DI water (~710 nm, reference wavelength) and L-tryptophan (~279 nm) and vitamin B12 (~360 nm) and lysozyme (~282 nm) were used to obtain a diffusive flux, and the ratio of the slopes of concentration with respect to time for the bare PCTE was used to compute the normalized flux

flow rate across PCTE + G + IP + O2 plasma flow rate across PCTE

ASSOCIATED CONTENT

5 Supporting Information

The Supporting Information is available free of charge at https://pubs.acs.org/doi/10.1021/acsami.2c10827.

Experimental setup used to test air flow through the nanoporous atomically thin graphene membranes; increase in system pressure as a function of time to check for baseline leakage rate; increase in system pressure as a function of time for (A) Bare PCTE, (B) PCTE with IP treatment, and (C) graphene on PCTE with IP membranes in the system; the influence of starting pressure on the rate of change of pressure for the three different types of membranes: PCTE, PCTE with IP, and graphene on PCTE with IP; calculated air permeance as a function of the size of nanoparticles filtered using graphene membranes in this work compared to commercial air filters; diffusive flux normalized with respect to bare PCTE support membrane for PCTE + G, PCTE + G + IP, and PCTE + G + IP + 60 s O₂ plasma membranes; and representative SEM images of the graphene membrane after SiO₂ nanoparticle filtration (PDF)

AUTHOR INFORMATION

Corresponding Author

Piran R. Kidambi — Department of Chemical and Biomolecular Engineering, Department of Mechanical Engineering, and Vanderbilt Institute of Nanoscale Sciences and Engineering, Vanderbilt University, Nashville, Tennessee 37212, United States; Orcid.org/0000-0003-1546-5014; Email: piran.kidambi@vanderbilt.edu

Authors

- Peifu Cheng Department of Chemical and Biomolecular Engineering, Vanderbilt University, Nashville, Tennessee 37212, United States
- Jeremy Espano Interdisciplinary Graduate Program for Material Science, Vanderbilt University, Nashville, Tennessee 37212, United States
- Andrew Harkaway Department of Mechanical Engineering, Vanderbilt University, Nashville, Tennessee 37212, United States
- Andrew E. Naclerio Department of Chemical and Biomolecular Engineering, Vanderbilt University, Nashville, Tennessee 37212, United States
- Nicole K. Moehring Department of Chemical and Biomolecular Engineering and Interdisciplinary Graduate Program for Material Science, Vanderbilt University, Nashville, Tennessee 37212, United States
- Philipp Braeuninger-Weimer Deep Science Fund, Intellectual Ventures, Seattle, Washington 98005, United States

Complete contact information is available at: https://pubs.acs.org/10.1021/acsami.2c10827

Funding

This work was supported in part by Intellectual Ventures, NSF CAREER award #1944134, and faculty start-up funds to P.R.K. from Vanderbilt University.

Notes

The authors declare the following competing financial interest(s): P.R.K. declares stake in a company aimed at commercializing application from 2D materials.

ACKNOWLEDGMENTS

We acknowledge the use of Vanderbilt Institute of Nanoscale Science and Engineering CORE facilities and Prof. Carlos Silvera Batista's Lab at Vanderbilt University for providing the silica nanoparticles.

REFERENCES

- (1) Abdolghader, P.; Brochot, C.; Haghighat, F.; Bahloul, A. Airborne Nanoparticles Filtration Performance of Fibrous Media: A Review. Sci. Technol. Built Environ. 2018, 24, 648–672.
- (2) Wang, J.; Tronville, P. Toward Standardized Test Methods to Determine the Effectiveness of Filtration Media against Airborne Nanoparticles. *J. Nanoparticle Res.* **2014**, *16*, 1–33.
- (3) Bortolassi, A. C. C.; Nagarajan, S.; de Araújo Lima, B.; Guerra, V. G.; Aguiar, M. L.; Huon, V.; Soussan, L.; Cornu, D.; Miele, P.; Bechelany, M. Efficient Nanoparticles Removal and Bactericidal Action of Electrospun Nanofibers Membranes for Air Filtration. *Mater. Sci. Eng. C* 2019, 102, 718–729.
- (4) de Almeida, D. S.; Martins, L. D.; Muniz, E. C.; Rudke, A. P.; Squizzato, R.; Beal, A.; de Souza, P. R.; Bonfim, D. P. F.; Aguiar, M. L.; Gimenes, M. L. Biodegradable CA/CPB Electrospun Nanofibers for Efficient Retention of Airborne Nanoparticles. *Process Saf. Environ. Prot.* 2020, 144, 177–185.
- (5) Liu, J.; Pui, D. Y. H.; Wang, J. Removal of Airborne Nanoparticles by Membrane Coated Filters. *Sci. Total Environ.* **2011**, 409, 4868–4874.
- (6) Lange, R.; Fissan, H.; Schmidt-Ott, A. Predicting the Collection Efficiency of Agglomerates in Fibrous Filters. *Part. Part. Syst. Charact.* **1999**, *16*, 60–65.
- (7) Schmid, S.; Kurek, M.; Adolphsen, J. Q.; Boisen, A. Real-Time Single Airborne Nanoparticle Detection with Nanomechanical Resonant Filter-Fiber. *Sci. Rep.* **2013**, *3*, 1–5.
- (8) Rezaei, M.; Johnson, M. S. Airborne Nanoparticles: Control and Detection. *Air Pollut. Sources, Stat. Heal. Eff.* **2021**, 85–133.
- (9) Biskos, G.; Schmidt-Ott, A. Airborne Engineered Nanoparticles: Potential Risks and Monitoring Challenges for Assessing Their Impacts on Children. *Paediatr. Respir. Rev.* **2012**, *13*, 79–83.
- (10) Gopinath, S. C. B.; Tang, T. H.; Chen, Y.; Citartan, M.; Tominaga, J.; Lakshmipriya, T. Sensing Strategies for Influenza Surveillance. *Biosens. Bioelectron.* **2014**, *61*, 357–369.
- (11) Verreault, D.; Moineau, S.; Duchaine, C. Methods for Sampling of Airborne Viruses. *Microbiol. Mol. Biol. Rev.* **2008**, 72, 413–444.
- (12) Wisdom, A.; Kutkowska, A. E.; Leitch, E. C. M. W.; Gaunt, E.; Templeton, K.; Harvala, H.; Simmonds, P. Genetics, Recombination and Clinical Features of Human Rhinovirus Species C (HRV-C) Infections; Interactions of HRV-C with Other Respiratory Viruses. *PLoS One* **2009**, *4*, No. e8518.
- (13) Shereen, M. A.; Khan, S.; Kazmi, A.; Bashir, N.; Siddique, R. COVID-19 Infection: Origin, Transmission, and Characteristics of Human Coronaviruses. *J. Adv. Res.* **2020**, *24*, 91–98.
- (14) Suen, L. K. P.; Guo, Y. P.; Ho, S. S. K.; Au-Yeung, C. H.; Lam, S. C. Comparing Mask Fit and Usability of Traditional and Nanofibre N95 Filtering Facepiece Respirators before and after Nursing Procedures. *J. Hosp. Infect.* **2020**, *104*, 336–343.
- (15) Ratnesar-Shumate, S.; Wu, C. Y.; Wander, J.; Lundgren, D.; Farrah, S.; Lee, J. H.; Wanakule, P.; Blackburn, M.; Lan, M. F. Evaluation of Physical Capture Efficiency and Disinfection Capability of an Iodinated Biocidal Filter Medium. *Aerosol Air Qual. Res.* **2008**, *8*, 1–18
- (16) Liu, W.; Liu, K.; Du, H.; Zheng, T.; Zhang, N.; Xu, T.; Pang, B.; Zhang, X.; Si, C.; Zhang, K. Cellulose Nanopaper: Fabrication, Functionalization, and Applications. *Nano-Micro Lett.* **2022**, *14*, 104.

- (17) Wartell, M.; Kleinman, M.; Huey, B. Strategies to Protect the Health of Deployed U.S. Forces; National Academies Press: Washington (DC), 1999.
- (18) Schreuder-Gibson, H. L.; Truong, Q.; Walker, J. E.; Owens, J. R.; Wander, J. D.; Jones, W. E. Chemical and Biological Protection and Detection in Fabrics for Protective Clothing. *MRS Bull.* **2003**, 28 (8), 574–578.
- (19) Lu, X.; Nguyen, V.; Zhou, M.; Zeng, X.; Jin, J.; Elliott, B. J.; Gin, D. L. Crosslinked Bicontinuous Cubic Lyotropic Liquid-Crystal/Butyl-Rubber Composites: Highly Selective, Breathable Barrier Materials for Chemical Agent Protection. *Adv. Mater.* **2006**, *18*, 3294–3298.
- (20) Hudiono, Y. C.; Miller, A. L.; Gibson, P. W.; LaFrate, A. L.; Noble, R. D.; Gin, D. L. A Highly Breathable Organic/Inorganic Barrier Material That Blocks the Passage of Mustard Agent Simulants. *Ind. Eng. Chem. Res.* **2012**, *51*, 7453–7456.
- (21) Jung, K. H.; Pourdeyhimi, B.; Zhang, X. Chemical Protection Performance of Polystyrene Sulfonic Acid-Filled Polypropylene Nonwoven Membranes. *J. Membr. Sci.* **2010**, *362*, 137–142.
- (22) Bulejko, P.; Krištof, O.; Dohnal, M.; Svěrák, T. Fine/Ultrafine Particle Air Filtration and Aerosol Loading of Hollow-Fiber Membranes: A Comparison of Mathematical Models for the Most Penetrating Particle Size and Dimensionless Permeability with Experimental Data. *J. Membr. Sci.* **2019**, *592*, 117393.
- (23) Chen, R.; Zhang, H.; Wang, M.; Zhang, X.; Gan, Z. Thermoplastic Polyurethane Nanofiber Membrane Based Air Filters for Efficient Removal of Ultrafine Particulate Matter PM0.1. ACS Appl. Nano Mater. 2021, 4, 182–189.
- (24) Zhang, S.; Tang, N.; Cao, L.; Yin, X.; Yu, J.; Ding, B. Highly Integrated Polysulfone/Polyacrylonitrile/Polyamide-6 Air Filter for Multilevel Physical Sieving Airborne Particles. ACS Appl. Mater. Interfaces 2016, 8, 29062–29072.
- (25) Datasheet of PCTE Membrane; Sterlitech https://www.sterlitech.com/hydrophobic-polycarbonate-membrane-filter-pctf0225100.html (accessed on May 5, 2022).
- (26) Bui, N.; Meshot, E. R.; Kim, S.; Peña, J.; Gibson, P. W.; Wu, K. J.; Fornasiero, F. Ultrabreathable and Protective Membranes with Sub-5 nm Carbon Nanotube Pores. *Adv. Mater.* **2016**, *28*, 5871–5877.
- (27) Holt, J. K.; Park, H. G.; Wang, Y.; Stadermann, M.; Artyukhin, A. B.; Grigoropoulos, C. P.; Noy, A.; Bakajin, O. Fast Mass Transport Through Sub-2-Nanometer Carbon Nanotubes. *Science* **2006**, *312*, 1034–1037.
- (28) El-Atab, N.; Qaiser, N.; Badghaish, H.; Shaikh, S. F.; Hussain, M. M.; Hussain, M. M. Flexible Nanoporous Template for the Design and Development of Reusable Anti-COVID-19 Hydrophobic Face Masks. *ACS Nano* **2020**, *14*, 7659–7665.
- (29) van den Bergh, J.; Zhu, W.; Gascon, J.; Moulijn, J. A.; Kapteijn, F. Separation and Permeation Characteristics of a DD3R Zeolite Membrane. *J. Membr. Sci.* **2008**, *316*, 35–45.
- (30) Wu, T.; Lucero, J.; Crawford, J. M.; Sinnwell, M. A.; Thallapally, P. K.; Carreon, M. A. SAPO-34 Membranes for Xenon Capture from Air. *J. Membr. Sci.* **2019**, *573*, 288–292.
- (31) Wang, L.; Williams, C. M.; Boutilier, M. S. H.; Kidambi, P. R.; Karnik, R. Single-Layer Graphene Membranes Withstand Ultrahigh Applied Pressure. *Nano Lett.* **2017**, *17*, 3081–3088.
- (32) Wang, L.; Boutilier, M. S. H.; Kidambi, P. R.; Jang, D.; Hadjiconstantinou, N. G.; Karnik, R. Fundamental Transport Mechanisms, Fabrication and Potential Applications of Nanoporous Atomically Thin Membranes. *Nat. Nanotechnol.* **2017**, *12*, 509–522.
- (33) Prozorovska, L.; Kidambi, P. R. State-of-the-Art and Future Prospects for Atomically Thin Membranes from 2D Materials. *Adv. Mat.* **2018**, DOI: 10.1002/adma.201801179.
- (34) Kidambi, P. R.; Nguyen, G. D.; Zhang, S.; Chen, Q.; Kong, J.; Warner, J.; Li, A.-P.; Karnik, R. Facile Fabrication of Large-Area Atomically Thin Membranes by Direct Synthesis of Graphene with Nanoscale Porosity. *Adv. Mater.* **2018**, *30*, 1804977.
- (35) Kidambi, P. R.; Terry, R. A.; Wang, L.; Boutilier, M. S. H.; Jang, D.; Kong, J.; Karnik, R. Assessment and Control of the

- Impermeability of Graphene for Atomically Thin Membranes and Barriers. *Nanoscale* **2017**, *9*, 8496–8507.
- (36) Kidambi, P. R.; Ducati, C.; Dlubak, B.; Gardiner, D.; Weatherup, R. S.; Martin, M.-B.; Seneor, P.; Coles, H.; Hofmann, S. The Parameter Space of Graphene Chemical Vapor Deposition on Polycrystalline Cu. *J. Phys. Chem. C* **2012**, *116*, 22492–22501.
- (37) Kidambi, P. R.; Bayer, B. C.; Blume, R.; Wang, Z.-J.; Baehtz, C.; Weatherup, R. S.; Willinger, M.-G.; Schloegl, R.; Hofmann, S. Observing Graphene Grow: Catalyst—Graphene Interactions during Scalable Graphene Growth on Polycrystalline Copper. *Nano Lett.* **2013**, *13*, 4769–4778.
- (38) Kidambi, P. R.; Jang, D.; Idrobo, J.-C.; Boutilier, M. S. H.; Wang, L.; Kong, J.; Karnik, R. Nanoporous Atomically Thin Graphene Membranes for Desalting and Dialysis Applications. *Adv. Mater.* **2017**, *29*, 1700277.
- (39) Cheng, P.; Kelly, M. M.; Moehring, N. K.; Ko, W.; Li, A.-P.; Idrobo, J. C.; Boutilier, M. S. H.; Kidambi, P. R. Facile Size-Selective Defect Sealing in Large-Area Atomically Thin Graphene Membranes for Sub-Nanometer Scale Separations. *Nano Lett.* **2020**, 20, 5951–5959.
- (40) Boutilier, M. S. H.; Sun, C.; O'Hern, S. C.; Au, H.; Hadjiconstantinou, N. G.; Karnik, R. Implications of Permeation through Intrinsic Defects in Graphene on the Design of Defect-Tolerant Membranes for Gas Separation. *ACS Nano* **2014**, *8*, 841–849.
- (41) O'Hern, S. C.; Jang, D.; Bose, S.; Idrobo, J.-C.; Song, Y.; Laoui, T.; Kong, J.; Karnik, R. Nanofiltration across Defect-Sealed Nanoporous Monolayer Graphene. *Nano Lett.* **2015**, *15*, 3254.
- (42) O'Hern, S. C.; Boutilier, M. S. H.; Idrobo, J.-C.; Song, Y.; Kong, J.; Laoui, T.; Atieh, M.; Karnik, R. Selective Ionic Transport through Tunable Subnanometer Pores in Single-Layer Graphene Membranes. *Nano Lett.* **2014**, *14*, 1234.
- (43) Wang, R.; Whelan, P. R.; Braueninger-Weimer, P.; Tappertzhofen, S.; et al. Catalyst Interface Engineering for Improved 2D Film Lift-Off and Transfer. ACS Appl. Mater. Interfaces 2016, 8 (48), 33072–33082.
- (44) Chaturvedi, P.; Moehring, N. K.; Cheng, P.; Vlassiouk, I.; Boutilier, M. S. H.; Kidambi, P. R. Deconstructing proton transport through atomically thin monolayer CVD graphene membranes. *J. Mater. Chem.* **2022**, Advance Article.
- (45) Ferrari, A. C.; Basko, D. M. Raman Spectroscopy as a Versatile Tool for Studying the Properties of Graphene. *Nat. Nanotechnol.* **2013**, *8*, 235–246.
- (46) Dalwani, M.; Zheng, J.; Hempenius, M.; Raaijmakers, M. J. T.; Doherty, C. M.; Hill, A. J.; Wessling, M.; Benes, N. E. Ultra-Thin Hybrid Polyhedral Silsesquioxane-Polyamide Films with Potentially Unlimited 2D Dimensions. *J. Mater. Chem.* **2012**, *22*, 14835–14838.
- (47) Kidambi, P. R.; Mariappan, D. D.; Dee, N. T.; Vyatskikh, A.; Zhang, S.; Karnik, R.; Hart, A. J. A Scalable Route to Nanoporous Large-Area Atomically Thin Graphene Membranes by Roll-to-Roll Chemical Vapor Deposition and Polymer Support Casting. *ACS Appl. Mater. Interfaces* **2018**, *10*, 10369–10378.
- (48) Zhang, Y.; Benes, N. E.; Lammertink, R. G. H. Visualization and Characterization of Interfacial Polymerization Layer Formation. *Lab Chip* **2015**, *15*, 575–580.
- (49) Duan, J.; Litwiller, E.; Pinnau, I. Preparation and Water Desalination Properties of POSS-Polyamide Nanocomposite Reverse Osmosis Membranes. *J. Membr. Sci.* **2015**, *473*, 157–164.
- (50) Childres, I.; Jauregui, L. A.; Tian, J.; Chen, Y. P. Effect of Oxygen Plasma Etching on Graphene Studied Using Raman Spectroscopy and Electronic Transport Measurements. *New J. Phys.* **2011**, *13*, 025008.
- (51) Surwade, S. P.; Smirnov, S. N.; Vlassiouk, I. V.; Unocic, R. R.; Veith, G. M.; Dai, S.; Mahurin, S. M. Water Desalination Using Nanoporous Single-Layer Graphene. *Nat. Nanotechnol.* **2015**, *10*, 459–464.
- (52) Vertegel, A. A.; Siegel, R. W.; Dordick, J. S. Silica Nanoparticle Size Influences the Structure and Enzymatic Activity of Adsorbed Lysozyme. *Langmuir* **2004**, *20*, 6800–6807.

- (53) Boutilier, M. S. H.; Jang, D.; Idrobo, J.-C.; Kidambi, P. R.; Hadjiconstantinou, N. G.; Karnik, R. Molecular Sieving Across Centimeter-Scale Single-Layer Nanoporous Graphene Membranes. ACS Nano 2017, 11, 5726-5736.
- (54) Weatherup, R. S.; Eren, B.; Hao, Y.; Bluhm, H.; Salmeron, M. B. Graphene Membranes for Atmospheric Pressure Photoelectron Spectroscopy. J. Phys. Chem. Lett. 2016, 7, 1622-1627.
- (55) Wang, F.; Tarabara, V. V. Pore Blocking Mechanisms during Early Stages of Membrane Fouling by Colloids. J. Colloid Interface Sci. 2008, 328, 464-469.
- (56) Koonani, H.; Amirinejad, M. Combined Three Mechanisms Models for Membrane Fouling during Microfiltration. J. Membr. Sci. Res. 2019, 5, 274-282.
- (57) Lowther, S. D.; Deng, W.; Fang, Z.; Booker, D.; Whyatt, D. J.; Wild, O.; Wang, X.; Jones, K. C. How Efficiently Can HEPA Purifiers Remove Priority Fine and Ultrafine Particles from Indoor Air? Environ. Int. 2020, 144, 106001.
- (58) Konda, A.; Prakash, A.; Moss, G. A.; Schmoldt, M.; Grant, G. D.; Guha, S. Aerosol Filtration Efficiency of Common Fabrics Used in Respiratory Cloth Masks. ACS Nano 2020, 14, 6339-6347.
- (59) Cheng, P.; Moehring, N. K.; Idrobo, J. C.; Ivanov, I. N.; Kidambi, P. R. Scalable Synthesis of Nanoporous Atomically Thin Graphene Membranes for Dialysis and Molecular Separations via Facile Isopropanol-Assisted Hot Lamination. Nanoscale 2021, 13, 2825-2837.
- (60) Kundrot, C. E.; Richards, F. M. Crystal Structure of Hen Egg-White Lysozyme at a Hydrostatic Pressure of 1000 Atmospheres. J. Mol. Biol. 1987, 193, 157-170.

□ Recommended by ACS

Layer-Dependent Nanowear of Graphene Oxide

Chuan Tang, Linmao Qian, et al.

FEBRUARY 03, 2023

ACS NANO

READ **Z**

Hygroelectric Generator Based on Antisymmetric Modification of Graphene Spheres with Ionic Hydrogels

Changbao Xu, Mingyong Xin, et al.

APRIL 05, 2023

ACS APPLIED NANO MATERIALS

READ **C**

Effect of Surface Treatment on Performance and Internal Stacking Mode of Electrohydrodynamic Printed Graphene and Its Microsupercapacitor

Jinyao Zhong, Junbiao Peng, et al.

JANUARY 04, 2023

ACS APPLIED MATERIALS & INTERFACES

READ **C**

Tunable Ion Transport with Freestanding Vermiculite Membranes

Zijing Xia, Seth B. Darling, et al.

NOVEMBER 01, 2022

ACS NANO

READ 2

Get More Suggestions >